J Mater Sci (2009) 44:5885–5893
DOI 10.1007/s10853-009-3832-x

Surface state charge dynamics in hydrazone-doped polyesters

D. M. Goldie

Received: 8 May 2009 / Accepted: 21 August 2009 / Published online: 2 September 2009

Abstract Electronic properties of surface states in hydrazone-doped polyesters (HDPs) have been investigated using a series of thin-film Au/HDP/Al diode structures. Controlled space-charge-limited hole injection from the Au ohmic electrode under forward-bias was used to charge surface states in the vicinity of the Al blocking electrode. Subsequent reverse-biasing of the diodes to extract the remaining surface charge after suitable delay intervals permitted the occupation dynamics of holes trapped in the surface states to be determined. The decay times for trapped holes are found to depend upon the level of hydrazone doping in the films and also the initial trap occupancy following forward-bias charging. A simple surface-leakage model in which the leakage mobility is dependent upon the local surface electric field is found to provide a good description of the experimental data. The leakage model suggests that the minimum density of surface states is 4×10^{12} cm^{-2} and that these states lie within about 17 Å of the film surface.

Introduction

Electronic devices that employ thin-film organic materials are becoming increasingly available in a diverse range of consumer products. For certain applications, such as large-area displays and optoelectronic imaging, organic materials offer significant commercial advantages over inorganic alternatives. These advantages are mainly achieved through simpler solvent-based processing of polymer materials and the consequent ability to batch-process products using roll-to-roll printing techniques [1–3]. A diverse range of polymers are presently used in organic products, where the electronic response of the various constituent layers may be controlled by chemical synthesis or chemical doping. An important class of organic materials is molecularly doped polymers [4] (MDPs). For MDPs, the electronic response is dictated by the amount of dopant material that is dispersed throughout an insulating polymer binder. The dopant materials are typically small oxidisable molecules such as hydrazones, amines or benzidines, with polycarbonates, polyesters or polystyrenes being used as binders. Electronic conduction in MDPs has been shown to proceed via charge carrier hopping between the dopant sites [4, 5].

An important application of MDPs is to function as a charge-transport layer in xerographic imaging systems [4, 6]. During xerographic imaging, the MDP is required to efficiently transfer charge across a film thickness of around 20–30 μm to produce a perfect electrostatic image on its free surface. To avoid unwanted hysteresis effects, the MDP should ideally not trap charge in either its bulk or surface region. Considerable effort has therefore been devoted to minimising the level of bulk trapping in MDPs by eliminating chemical impurities through improved synthesis procedures. The success of these synthesis modifications has been demonstrated through the observation of trap-free space-charge-limited current (SCLC) behaviour in several MDPs [7–9]. Noticeably, less attention has been expended towards investigating surface-trapping in MDPs, where only indirect evidence that the surface region contains significantly high trap densities relative to the bulk has been inferred by charge transport modelling [10–12]. This may reflect the experimental complexity of performing meaningful surface charge measurements under controlled ambient conditions. An

D. M. Goldie (✉)
Division of Electronic Engineering and Physics, University of Dundee, Perth Road, Dundee DD1 4HN, Scotland, UK
e-mail: d.m.goldie@dundee.ac.uk

alternative experimental approach towards characterising MDP surface states is therefore proposed in this study. The technique uses an MDP diode configuration, identical to that used in previous SCLC studies [7–9], to provide simple charge probing of the surface states.

Experimental details

The MDP studied was a hydrazone-doped polyester (HDP). The hydrazone, *p*-diethylaminobenzaldehyde-1,1′-diphenylhydrazone (DEH), was obtained in a purified form and used as-received. The polyester (PE) was purchased from a commercial supplier (trade name VITEL 200) and used as-received. Thin-films of the HDP were deposited by spin-coating from dichloromethane solutions that contained weighed amounts of DEH and PE. The amount of hydrazone in the cast films was taken to be equal to the concentration by weight (C_w) of DEH to PE in the prepared dichloromethane solutions. Films were prepared using $10\% \leq C_w \leq 50\%$. The films were coated onto glass substrates fitted with patterned gold electrodes. A thin layer of chromium was used to improve the adhesion properties of the gold to the glass. Following a drying period of a few days at room temperature to allow residual solvent to evaporate, a patterned layer of aluminium was finally evaporated onto the top surface of the films to complete a Cr/Au/HDP/Al device structure as depicted in Fig. 1. The active device area defined by the patterned Au and Al contacts was 0.16 cm^2. A summary of the prepared specimens is given in Table 1, where the thicknesses (L) of the HDP films were determined using a surface profilimeter.

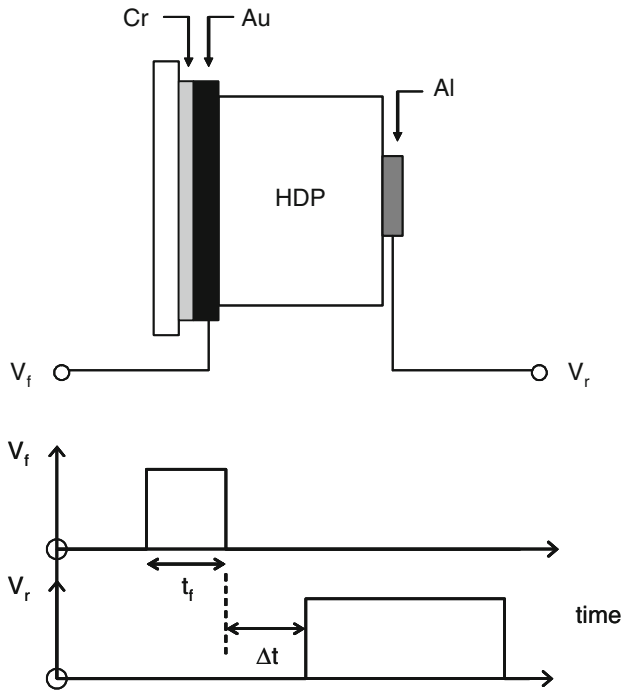

Fig. 1 HDP specimen configuration and voltage–pulse sequence used for experiments. *G* glass substrate, V_f forward voltage, V_r reverse voltage, t_f forward injection time; Δt delay time

Charge probing of states in the vicinity of the Al contact was performed using the voltage–pulse sequence illustrated in Fig. 1. A forward pulse of duration t_f and magnitude V_f was first applied to the Au injection contact to establish a controlled space-charge-limited (SCL) current flow of holes throughout the HDP bulk. These injected holes were used to charge states in the vicinity of the Al extraction electrode. The amount of hole charge trapped in these states was then measured by sweeping these holes out of the film via the Au contact through the application of a reverse pulse of duration t_r and magnitude V_r to the Al blocking electrode. A finite delay time Δt was allowed to elapse between the end of the V_f charging pulse and the start of the V_r collection pulse. The minimum value of Δt ($\sim$5 s) was dictated by the experimental arrangement used to manually switch from V_f to V_r. The voltage pulses were generated using a proprietary p-Mosfet switch configuration powered from a stabilised high-voltage supply. This arrangement was capable of generating high-voltage pulses up to 400 V with an associated rise time of less than 50 μs. For the majority of measurements performed, V_r was set equal to V_f. The generated current signals under either V_f or V_r stimulation were pre-amplified and recorded on a 100-MHz digital oscilloscope before being transferred to a computer for analysis. For most experiments, the HDP specimens were held in a shielded light-tight box under ambient room temperature (295 K) conditions. Some limited temperature studies were also performed, where the specimens were mounted in a light-sealed liquid nitrogen

Table 1 HDP samples used in this study

$\rho = (M_w/A_v d C_w)^{1/3}$ where A_v = Avogadro's constant and for DEH $M_w = 343$ g mol^{-1}, $d = 1.12$ g cm^{-3}. The μ_0, β and m parameters have been obtained at a temperature of 295 K

Sample code	L (μm)	C_w (%)	ρ (Å)	μ_0 (cm^2 V^{-1} s^{-1})	β ($\times 10^{-3}$) ($cm^{½}$ $V^{-½}$)	m
HDP1	4.2 ± 0.3	10	17.2	$2.8 \pm 1.0 \times 10^{-11}$	4.5 ± 0.2	3.52 ± 1.10
HDP2	3.0 ± 0.2	20	13.7	$1.5 \pm 0.2 \times 10^{-9}$	4.3 ± 0.2	1.74 ± 0.12
HDP3	5.9 ± 0.3	30	11.9	$9.7 \pm 1.8 \times 10^{-9}$	4.7 ± 0.1	1.84 ± 0.09
HDP4	4.6 ± 0.1	40	10.9	$4.1 \pm 0.3 \times 10^{-8}$	4.5 ± 0.2	1.67 ± 0.07
HDP5	6.9 ± 0.2	50	10.1	$7.3 \pm 0.3 \times 10^{-8}$	4.3 ± 0.2	0.93 ± 0.05

bath cryostat that used dry helium as a thermal exchange gas.

Results and discussion

Previous study using Cr/Au/HDP/Al diodes has demonstrated that the transient current pulse under forward bias is consistent with the injection of hole carriers from the Au electrode into the HDP bulk [7, 8, 13]. Examples of such forward injection pulses are included in Fig. 2 for specimen HDP3. The forward injection transient attains a maximum overshoot at a time t_p following the application of V_f which corresponds to the arrival of the leading edge of the injected hole charge sheet at the Al extraction electrode. The associated hole mobility μ_h may then be estimated from $\mu_h = cL^2/(V_f \cdot t_p)$, where $c \sim 0.8$ in the absence of charge carrier diffusion. For a fixed temperature, the calculated mobility values are found to increase with the strength of the applied ohmic electric field F_Ω (=V_f/L) and may be parameterised by a phenomenological Poole–Frenkel description such that;

$$\mu_h = \mu_0 \cdot \exp\left(\beta \cdot \sqrt{F_\Omega}\right) \quad (1)$$

The μ_0 and β parameters that characterise the HDP samples used in this study are given in Table 1. The underlying microscopic model that is commonly used to interpret Eq. 1 is based upon charge carrier hopping between the molecular dopant sites which are subject to both energetic and spatial disorder [14]. To produce Poole–Frenkel behaviour at lower values of F_Ω, it is furthermore essential that the energetic hopping landscape is spatially correlated [15]. Within the disordered hopping model, the measured β values are then expected to reflect the relative amounts of energetic to spatial disorder present for the DEH sites and from Table 1 this appears to be fairly constant across the doping range studied. In contrast, the parameter μ_0, which characterises the mobility under vanishing electric field when disorder effects are effectively removed, is highly sensitive to the DEH doping level and the associated centre-to-centre inter-site doping distance ρ. Estimates of ρ based upon the DEH molecules having a simplifying cubic shape are included in Table 1. A detailed analysis of the dependence of μ_0 upon ρ reveals that the charge transport mechanism is consistent with hole hopping between the DEH sites [16].

For times greater than about three or four times t_p, the forward current transient is observed to settle down to a steady-state magnitude. The voltage dependence of the steady-state current density (J_f) has previously been shown [7] to be consistent with the theoretical trap-free SCLC response at room temperature. The Au electrode therefore functions as an ohmic contact [8] so that if the relative permittivity of the HDP is ε_r and μ_h is given by Eq. 1

$$J_f \approx \mu_h \cdot \varepsilon_0 \cdot \varepsilon_r \cdot \frac{V_f^2}{L^3} \quad (2)$$

In contrast, low work-function metals, such as Al, exhibit blocking behaviour [7, 8] and are only capable of injecting currents which are significantly smaller than J_f by several orders of magnitude. The Cr/Au/HDP/Al diodes listed in Table 1 therefore provide an ideal device configuration to first control the injection of hole charge via J_f into the HDP bulk (V_f applied to Au electrode in Fig. 1) and to then measure how much of this injected charge may be recovered by subsequently applying a reverse-bias sweep-out pulse (V_r applied to Al electrode in Fig. 1). Similar experiments have previously been performed on anthracene crystals [17] to measure the amount of bulk space charge that remained following fast-switching between V_f and V_r ($\Delta t \rightarrow 0$ in Fig. 1). For the present HDP work, Δt is considered to be sufficiently long; however, that any remaining free bulk charge following

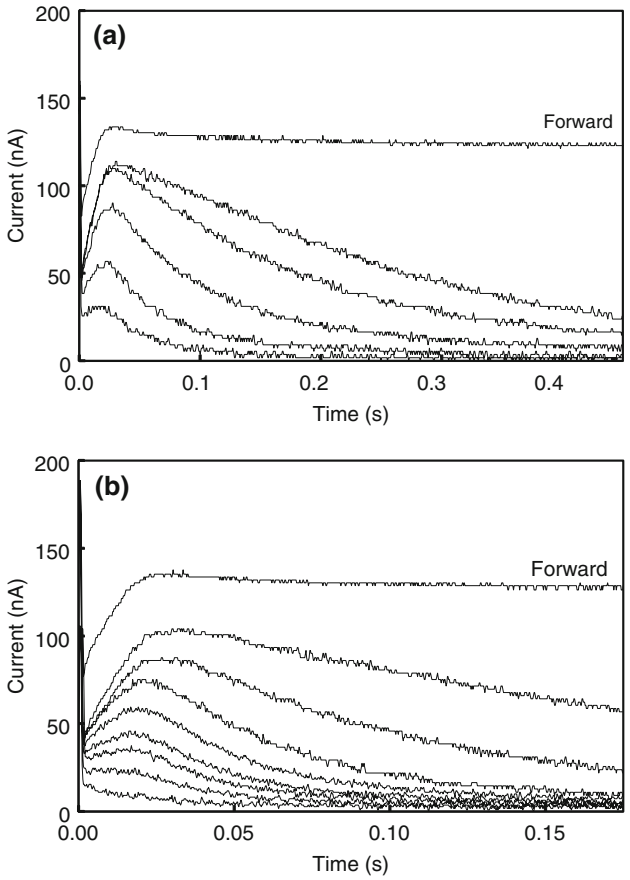

Fig. 2 Injected current pulse shapes at 295 K for sample HDP3 where $V_f = V_r = 120$ V. **a** $t_f = 1$ s. Δt values (s) decreasing from bottom signal were 300, 100, 30, 10 and 5. **b** $\Delta t = 10$ s. t_f values (ms) increasing from bottom signal were 10, 20, 30, 40, 60, 100, 250 and 1000. The current signal obtained under forward bias is labelled

injection is negligible and the collected charge thus represents hole carriers which are trapped during their passage from the Au to Al electrodes. The proposed trapping of holes is believed to occur mainly at states near the Al contact and evidence to support this is provided by a detailed examination of the transient current signals that are generated under reverse bias.

Reverse-bias pulse shapes

The origin of the hole charge that is collected under reverse-bias conditions is revealed by examining the associated transient current pulse shapes. Examples of such pulse shapes are given in Fig. 2 for sample HDP3. To obtain these signals, an amount of hole charge was first injected into the HDP bulk using a strong forward bias of $V_f = 120$ V for the stated duration times t_f. Following this injection period, transient current pulses under a reverse bias V_r were recorded for two distinct conditions. For the first set of pulses (Fig. 2a), the injection time t_f was held fixed at 1 s and signals were recorded for various delay times Δt between V_f and V_r. For the second set of pulses (Fig. 2b), the delay time Δt was held fixed at 10 s and the effect of varying t_f upon the reverse signals was recorded. Under both of these conditions, the reverse current pulse shapes are observed to display very similar features which can be summarised as follows:

(i) when the amount of collected charge (Q_r) under reverse bias is large, the reverse current pulses have a distinct peaked shape with the maximum coinciding very close to t_p in the forward injection pulse;
(ii) for low Q_r the reverse current pulses appear to attain a constant plateau response for times less than t_p.

The above characteristics are reminiscent of the type of signals that would be expected from a time-of-flight (TOF) experiment [18] if the reverse-biased Al contact were optically transparent and exposed to a short-duration pulse of strongly absorbed light. Under these circumstances, the ensuing transient photocurrent pulse shape is strongly influenced by the amount of photo-generated charge (Q_{pg}) relative to CV_r where C is the sample capacitance. For normal small-signal TOF conditions ($Q_{pg} \leq 0.05\ CV_r$), transient photo-currents in HDPs are indeed found to display a constant plateau region prior to charge extraction and the average carrier transit-time is comparable to t_p [13]. However, as the level of photo-generated charge becomes comparable to CV_r the current in the pre-extraction regime is found to increase with time due to space charge, and may accurately be described using an SCL finite-reservoir analysis [19]. For sample HDP3, the capacitance is estimated to be 72 pF taking $\varepsilon_r = 3$ so that $CV_r = 8.6$ nC. A gradual transition of the shape of the reverse-bias signal towards that which is characteristic of a small-signal TOF pulse is thus expected to be observed as Q_r is reduced below CV_r. Inspection of the $\Delta t = 300$ s signal in Fig. 2a (where $Q_r = 2.9$ nC) and the $t_f \leq 30$ ms signals in Fig. 2b (where $Q_r \leq 2.5$ nC) lend support to this anticipated-shape transition where the levels of current overshoot have become less noticeable.

The reverse-bias signals in Fig. 2 are therefore consistent with the re-injection of hole charge into the HDP bulk from a narrowly defined region near the Al contact. Since the Al contact is fundamentally blocking, this suggests that some of the holes that are injected during forward bias become trapped near the Al contact to form a spatially thin charge reservoir. Holes trapped in these reservoir states would then be available for release upon the application of V_r to produce the observed reverse-bias signals. The amount of charge that is available for re-injection from the proposed reservoir may be controlled by varying Δt (Fig. 2a) or t_f (Fig. 2b) and this influences the resulting -pulse shape in a similar manner to that discussed for the TOF photocurrents. Controlling Q_r in the HDP diodes by varying Δt or t_f during forward injection charging of the reservoir states is thus effectively equivalent to altering Q_{pg} in TOF experiments using optical filtering.

In evaluating the reverse-bias signal shapes seen in Fig. 2, it is important to consider the potential effect of any free hole charge that may be present throughout the HDP bulk. Free charge is (non-uniformly) distributed throughout the bulk once steady-state SCLC conditions have been established with the total amount lying between CV_f and $2CV_f$ [19]. This bulk charge, in addition to any surface-state trapped charge, will accordingly be present in Q_r as $\Delta t \rightarrow 0$ and will affect the associated reverse pulse shapes via non-uniformity of the internal electric field. Such electric field non-uniformity is most likely to be detected under small-signal re-injection conditions when the bulk and injected charges are comparable. The equivalent plateau shapes of the transient re-injection signals and TOF photocurrents (where there is no bulk charge present prior to photo-generation) are strong evidence that significant amounts of bulk charge are not present during the reverse-bias experiments. It would therefore appear that during the relatively long Δt intervals used in this study, charge introduced into the HDP bulk during forward injection is effectively removed either by a hole carrier recombination mechanism and/or by diffusion of free hole carriers to the diode contacts. The absence of significant bulk charge in HDP films contrasts with the situation reported for conjugated polymers [20] where high charge trapping at the metal–polymer interface is accompanied by a build-up of bulk space charge of opposite polarity.

Reservoir state charge dynamics

Useful information concerning the properties of the HDP reservoir states was obtained by studying the occupation dynamics of the trapped holes. This was most easily performed by investigating the rate of charge decay from the reservoir states. From Fig. 2a, it is noted that the amount of collected charge Q_r is strongly dependent upon the delay time Δt. Assuming that holes are promptly extracted from the reservoir states upon application of V_r, and experience no further losses upon traversing the HDP bulk, Q_r should provide an accurate measure of the amount of reservoir state holes that remain after a time Δt from an initially charged condition. The functional dependence of $Q_r(\Delta t)$ may then provide insight into physical mechanisms, such as surface charge leakage, that lead to the decay of trapped holes.

A series of measurements were therefore conducted to determine Q_r as a function of Δt for each of the HDP specimens. To allow a meaningful comparison of the $Q_r(\Delta t)$ data for different doping concentrations, the measurements were performed by ensuring that the reservoir states of all samples were initially fully charged at the start of the decay interval Δt. The requirement for saturation of the reservoir states was fulfilled, providing the total amount of hole charge injected during forward biasing was in excess of around 1700 nC cm^{-2}. For any particular specimen, V_f was accordingly selected to ensure that J_f exceeded a minimum value of about 1.6×10^{-6} A cm^{-2} for $t_f \geq 1$ s. From the initial saturated state, the collected charge Q_r was found by numerical integration of the recorded reverse-bias current signals for various Δt. Corrections to Q_r were applied to remove the inherent reverse capacitive switching contribution which was always present even when the reservoir states were fully depopulated. The reverse switching contribution became increasingly important for smaller values of Q_r when Δt was long.

The results of the $Q_r(\Delta t)$ measurements are given in Fig. 3. The data are presented on a double-logarithmic scale to accommodate the wide range of Q_r values encountered across the specimen doping range. The most striking feature of Fig. 3 data is the general tendency for the rate of reservoir hole decay to increase as the DEH doping level becomes greater. Curiously, however, the decay rate appears to be rather insensitive to doping over a fairly broad range when $20\% \leq C_w \leq 40\%$. Possible reasons for this phenomenon are discussed later. The other important artefact suggested from Fig. 3 is that the reservoir state charge decay follows a simple power–law dependence upon time. For the restricted range of Δt experimentally accessible, the optimum power–law fits to the data are indicated in Fig. 3 by the dashed lines. Extrapolation of these fitted lines to lower Δt suggests that they intersect at a common focal point when $\Delta t \sim 0.1$ s and $Q_r \sim 1640$ nC cm^{-2}. A possible reservoir state charge-leakage model that may explain these power–law observations is explored in the following section.

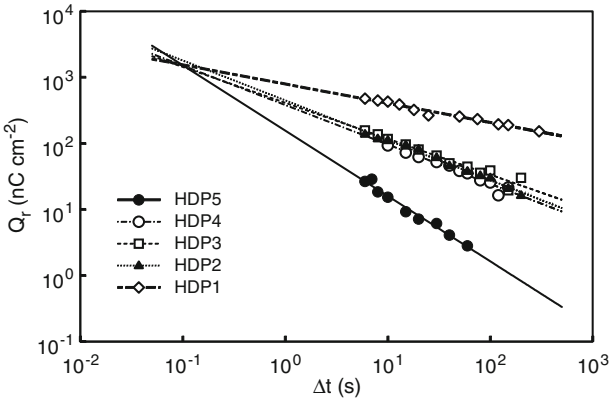

Fig. 3 Variation of collected charge with delay time for various weight concentrations C_w at 295 K. The values of V_f and t_f were chosen to ensure that the surface traps were initially fully occupied at the start of the delay period

Reservoir-state charge-leakage modelling

The phenomenological decay of the HDP reservoir charge with time indicates that trapped hole carriers are discharged via an available charge leakage path. Possible leakage paths involve either the release of trapped holes which return to the Au electrode, or the neutralisation of trapped holes by an electron current in the vicinity of the Al contact. The hole release and return mechanism would reintroduce space charge into the HDP bulk, however, and such space charge does not appear to exist as noted from the shape of the reverse currents under low-level injection conditions (section "Reverse-bias pulse shapes"). Furthermore, although a faster rate of discharge would be expected at higher doping levels if the holes were indeed returning to the Au contact, the discharge rate would then be expected to display a progressive increase with C_w. As previously noted (section "Reservoir state charge dynamics") this is not seen in Fig. 3 data for intermediate doping levels. From these collective arguments, it is anticipated that the discharge mechanism is more likely to involve an electron current that flows in the vicinity of the Al contact.

The leakage paths identified above are conveniently distinguished by the direction of the current flow during the delay interval Δt. In practice, the actual measurement of the discharge current is not straightforward since sufficiently long delay intervals must be allowed to elapse to ensure that there is no interference from the removal of free bulk space charge. For longer delays, the remaining reservoir discharge current is then expected to be small (<1 nA for $\Delta t > 5$ s) and outside the sensitivity of the experimental setup described in section "Experimental

details". An experimental determination of the reservoir discharge current direction therefore required the use of a source-measure unit with an estimated current sensitivity of about 0.1 pA. For a selection of samples, the current direction at $\Delta t = 10$ s indicated that the remaining trapped holes were indeed being discharged at the Al contact.

To model the dynamics of the removal of reservoir charge, it is thus necessary to first develop an expression for the inferred electron leakage current density J_L. If the population of holes in reservoir states per unit area is p_s, the time dependence of p_s in the presence of J_L may then be calculated from;

$$e \cdot \frac{dp_s}{dt} = -J_L \tag{3}$$

In Eq. 3, e denotes the fundamental unit of electronic charge. To proceed further it is necessary to speculate upon the physical nature of J_L. The leakage current occurs in close proximity to the Al electrode and is driven by the local surface electric field F_s. From Gauss's law, the surface field F_s will depend upon p_s and for a spatially thin density of reservoir states can be expressed as;

$$F_s = \frac{e \cdot p_s}{\varepsilon_0 \cdot \varepsilon_r} \tag{4}$$

From the magnitude of the saturated charge densities found from the $Q_r(\Delta t)$ data, F_s may readily exceed 10^6 V cm^{-1}. This surface field will drive J_L and it is recognised that there are two possible sources of electron charge for the discharge current; background electrons which are intrinsic to the HDP, and any extrinsically injected carriers from the Al contact. The electron injection capabilities of the Al contact are unknown, but an estimate of the discharge current magnitudes that are required may be performed by applying Eq. 3 to the $Q_r(\Delta t)$ data at experimentally accessible delay times. These calculations reveal that the overall HDP bulk conductivity would need to have a value of around 10^{-15} $(\Omega\ \text{cm})^{-1}$ if driven by the associated surface field F_s. This conductivity magnitude is typical for polyester materials [21] and implies that electron injection from the Al contact does not significantly perturb the background electron density. The adoption of a simplified discharge current model, which is based upon electron transport through the HDP bulk, would therefore appear reasonable where only the drift component is retained owing to the high surface field strengths. Denoting the available intrinsic concentration of electrons which drift under the influence of F_s as n, and the associated electron mobility by μ_e, J_L may then be expressed as

$$J_L = n \cdot e \cdot \mu_e \cdot F_s \tag{5}$$

For the wide range of surface electric fields which will exist during discharge of the reservoir states, the electron mobility may itself depend upon F_s. To accommodate this possibility, yet maintain analytical tractability, it is helpful to express μ_e in a simple power–law format whereby the mobility is reduced for weaker fields according to

$$\mu_e = \mu_e^0 \cdot \left(\frac{F_s}{F_\mu}\right)^m \tag{6}$$

In Eq. 6, $m > 0$ and the parameters μ_e^0 and F_μ are undetermined constants. Using the modelling information contained in Eqs. 5 and 6 for J_L, Eq. 3 may subsequently be solved to derive an explicit expression for the time dependence of p_s. The expression found for $p_s(t)$ is most usefully represented as

$$p_s(t) = p_s(0) \cdot \left[1 + m \cdot \left(\frac{F_s(0)}{F_\mu}\right)^m \cdot \frac{t}{\tau}\right]^{-\frac{1}{m}} \tag{7}$$

In Eq. 7, $p_s(0)$ is the concentration of holes in reservoir states at time $t = 0$, and $F_s(0)$ is the corresponding surface electric field from Eq. 4. The quantity τ in Eq. 7 is an effective screening time that depends upon the electron concentration n and is calculated as

$$\tau = \frac{\varepsilon_0 \cdot \varepsilon_r}{n \cdot e \cdot \mu_e^0} \tag{8}$$

To compare the $p_s(t)$ expression developed in Eq. 7 with the $Q_r(\Delta t)$ data presented in Fig. 3, it is first noted that for long delay times ($\Delta t \gg [\tau/m][F_\mu/F_s(0)]^m$) $p_s(t)$ may be approximated as

$$p_s(t) \approx p_s(0) \cdot m^{-\frac{1}{m}} \cdot \left(\frac{F_\mu}{F_s(0)}\right) \cdot \left[\frac{t}{\tau}\right]^{-\frac{1}{m}} \tag{9}$$

Equation 9 is immediately seen to have the required power–law dependence that is present in Fig. 3 data and the fitted power–law lines should thus provide information about the underlying mobility field-strength parameters m in Eq. 6. Furthermore, when $t = \tau$, Eq. 9 predicts that $p_s(\tau)$ will attain a value $p_s(0)[F_\mu/F_s(0)]m^{-(1/m)}$. Since $m^{-(1/m)}$ is only weakly dependent upon m, $p_s(\tau)$ is anticipated to show little variation for the specimen data in Fig. 3 provided that $p_s(0)$ (and hence $F_s(0)$) have well-defined values, independent of C_w, for initial saturated charging. The power–law $p_s(t)$ curves from Eq. 9 are consequently expected to converge at an approximate focal point when $t = \tau$ which is observed in Fig. 3 as previously noted.

The proposed surface-leakage model therefore appears to be consistent with the experimental results for $\Delta t \gg \tau$ when Eq. 9 may be applied to obtain approximate values for the mobility m-parameters and screening time τ. However, to obtain more accurate values for these model parameters, and in particular to find an estimate for the total density of reservoir states from $p_s(0)$, it is necessary to apply Eq. 7 which is applicable for all times. This presents a problem when it is realised that the selection of unique

fitting parameters may only be accomplished if $Q_r(\Delta t)$ data are available at shorter times that lie out with the power–law behaviour regime. It is nevertheless possible to quantify the limits for some of the leakage parameters which provide an acceptable fit of Eq. 7 to the $Q_r(\Delta t)$ data. The fitting procedure that was adopted first involved the application of Eq. 9 to the power–law regime to obtain estimates for the m-parameters, τ and the composite quantity $p_s(0)[F_\mu/F_s(0)]$ as described earlier. These initial estimates were then used in Eq. 7 under the constraint that independently assigned values for $p_s(0)$ and $[F_s(0)/F_\mu]$ satisfied the composite $p_s(0)[F_\mu/F_s(0)]$ estimate. An example of the fitting procedure is given in Fig. 4 using the parameters stated. The fitting of Eq. 7 resulted in a well-specified set of m-parameters which are summarised in Table 1, and gave a value for τ of 0.1 s. It is interesting to note that the deduced value for τ is very similar to independently measured bulk lifetime values ($\sim$30 ms) determined in DEH-doped polyester films by interrupted TOF measurements [22]. The similarity of the screening and lifetime values, both of which depend upon the local electron density, further supports the view that the local electron concentration is not significantly enhanced by injection near the Al contact and that the adoption of Eq. 5 to model J_L is justified.

In contrast, considerable flexibility was found concerning acceptable values for $p_s(0)$ and $[F_s(0)/F_\mu]$ provided the composite ratio of these parameters was fixed at 2050 nC cm^{-2}. The minimum value of $p_s(0)$ which gave an acceptable fit was found to be about 683 nC cm^{-2} for which $[F_s(0)/F_\mu] = 0.33$. Since $p_s(0)$ represents the amount of saturated hole charge held in reservoir states, the corresponding minimum reservoir state density is accordingly estimated to be $p_s(0)/e = 4 \times 10^{12}$ cm^{-2}. This magnitude is comparable to that found for other polymers which display weak surface electroluminescence [23] and interface state values estimated for polymer devices such as field-effect transistors [24] and metal–insulator–semiconductor capacitors [25].

Further support for the surface-leakage model is obtained by applying Eq. 7 to $Q_r(\Delta t)$ data under circumstances, where the reservoir states are only partially charged during forward injection. Partial charging was experimentally achieved by either (a) lowering V_f and hence J_f for a fixed t_f or (b) using a shorter t_f whilst keeping V_f and hence J_f fixed. Results obtained using both of these approaches are presented in Fig. 5 for specimen HDP3. For both sets of data, it is found that partial charging does not permit $Q_r(\Delta t)$ to be accurately described using a simple power–law response. Equation 9 is thus not applicable since for short delay times the criteria that $\Delta t \gg [\tau/m][F_\mu/F_s(0)]m$ is no longer fulfilled. The breakdown of Eq. 9 is a direct consequence of the lower reservoir charge density $p_s(0)$ and surface electric field $F_s(0)$. The use of partial charging therefore provides a critical test of Eq. 7 since the $p_s(0)$ and $F_s(0)/F_\mu$ parameters should scale by the same reservoir state occupancy factor when fitting the data sets in Fig. 5. Optimum fitting by Eq. 7 is indicated in Fig. 5 by the dashed curves. The fitted curves shown were generated

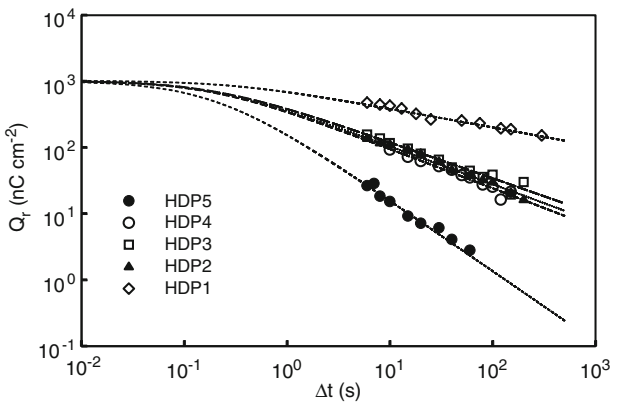

Fig. 4 Fit of collected charge data to Eq. 7 using the m values in Table 1. The other fitting parameters were $p_s(0) = 1025$ nC cm^{-2}, $F_s(0)/F_\mu = 0.5$ and $\tau = 0.1$ s

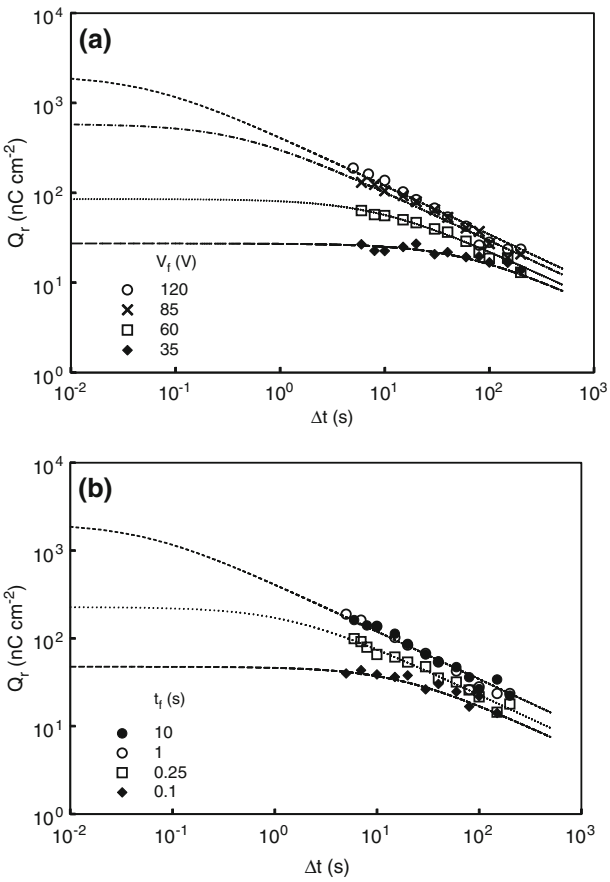

Fig. 5 Variation of collected charge with delay time at 295 K for sample HDP3 **a** $t_f = 1$ s, V_f (=V_r) variable as stated **b** V_f (=V_r) = 120 V, t_f variable as stated

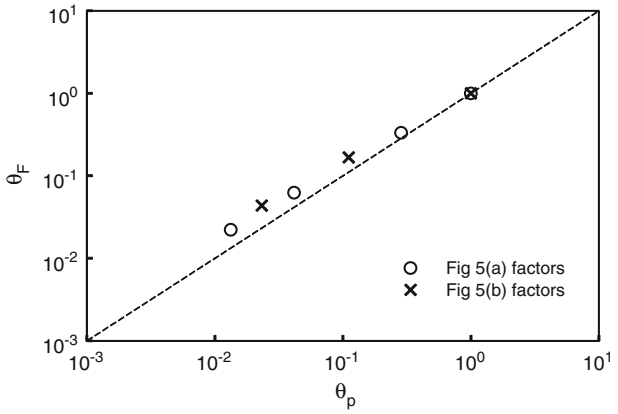

Fig. 6 Plot of surface state occupancy factors θ_F against θ_p found from the fitting procedure used in Fig. 5. The *dashed line* is a guide for the eye that shows $\theta_F = \theta_p$

by allowing $p_s(0)$ and $F_s(0)/F_\mu$ to be independently scaled by reservoir state occupancy factors θ_p and θ_F, respectively. The θ_p and θ_F occupancy factors used in the fits are finally plotted against each other in Fig. 6, where it is found that $\theta_F \sim \theta_p^{0.9}$. Lighter scaling of $F_s(0)/F_\mu$ therefore becomes increasingly necessary as $p_s(0)$ is progressively reduced so that, although Eq. 7 is capable of explaining the main behaviour exhibited in Fig. 5, it does possess some numerical limitations. The numerical restriction is presumably attributable to the simplified form for μ_e assumed in Eq. 6 where F_μ is taken to be constant.

Reservoir-state origin and location

The ability to fit the data in Fig. 4 using a common $p_s(0)$ value for all C_w indicates that the reservoir states are not influenced by the DEH dopant but originate in the polyester binder. This observation provides strong evidence that the reservoir states are associated with surface states that are intrinsic to the polyester and are not provided by DEH sites that act as effective traps due to field confinement near the Al electrode during Δt. Polymer surface states are anticipated to exist from numerous mechanisms including broken chains [26], surface defects caused by oxidation products [27] and localised fluctuations in the surface potential due to polarisation [28]. The use of alternative polymer binders might therefore be expected to result in different estimates of the density of surface states from $Q_r(\Delta t)$ measurements. Preliminary studies using either polycarbonate or polystyrene binders with $Cw = 50\%$ DEH indicates that $p_s(0)$, and hence the overall density of surface states, is generally larger by around a factor of two to three times the polyester magnitude. Further study on these binders is presently being conducted as well as an exploration of whether surface state densities are influenced by the type of dopant molecule for a given binder.

Although the DEH dopant does not determine the surface state density it does nevertheless have a strong influence upon the discharge rate of holes from these states. For the proposed charge-leakage model, this is to some extent unexpected as the proposed electron leakage current in the vicinity of the Al contact is not envisaged to involve DEH sites. However, if the surface states are distributed within a finite distance δ of the Al contact, then any DEH molecules in this region may possibly assist J_L by acting as intermediary electronic transport sites. The de-trapping of surface state charge to such DEH sites is expected to enhance J_L as the released holes will now lie closer to the Al contact. The discharge assistance offered by the dopant molecules should accordingly be sensitive to C_w which is reflected in the underlying mobility m-parameters given in Table 1 where faster discharge (smaller m) is found as C_w is increased and the importance of DEH within the surface state region δ is enhanced.

It is instructive to plot the room temperature m-parameters as a function of the average DEH separation distance ρ as shown in Fig. 7. As already noted, given the experimental uncertainty estimated for m, the data appear to define three distinct regions (marked as I, II and III in Fig. 7). The underlying nature of the leakage current that is associated with regions I–III is summarised in Table 2 and depends upon how ρ compares to δ and the effective size r_d

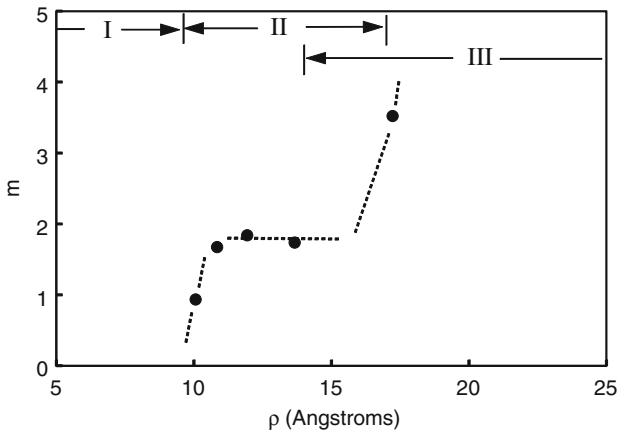

Fig. 7 Variation of mobility m-parameters with average DEH separation distance ρ

Table 2 Proposed current leakage mechanisms for regions I, II and III identified in Fig. 7

Region	Criteria	Leakage mechanism
I	$\rho \leq r_d$	DEH short
II	$r_d < \rho \leq \delta$	DEH assisted
III	$\rho > \delta$	DEH unassisted

(~8 Å for the cubic approximation [16]) of the DEH molecule itself. Region I corresponds to high doping levels where the average distance between DEH molecules becomes comparable to their actual size. For such high doping, the DEH molecules provide an efficient leakage short that allows de-trapped holes to be efficiently transported to the Al contact. As C_w is reduced (region II), the DEH molecules become well separated so that the DEH short is removed and there is a discontinuous change of m at the boundary between regions I and II. In region II DEH molecules continue to be important to the leakage process provided, there is at least one molecule per surface state within δ. If δ is of the order of a few r_d, the dependence of m in this region is not expected to be strongly dependent upon ρ as only a few DEH sites may participate to further displace holes closer to the Al electrode following initial de-trapping. However, as the doping level is reduced further and ρ exceeds δ (region III), a more significant shift in m is expected as there will now exist on average less than one DEH molecule per surface state within δ. The contribution of DEH to the leakage current is now severely diminished in region III. The boundary between regions II and III should therefore provide an estimate of δ and from Fig. 7 appears to occur when 14 Å $< \rho <$ 17 Å. To define δ more accurately, additional m data are required for C_w between 10 and 20% but the present range appears to represent a reasonable magnitude for the spatial depth of polymer surface states.

Although the analysis of the $Q_r(\Delta t)$ data is capable of providing useful information concerning the total surface state density, and to a limited extent the spatial location of these states, it is fundamentally unable to provide insight into how the surface states may be energetically distributed. Any energetic distribution of the surface states relative to the highest occupied molecular orbital (HOMO) of neighbouring DEH sites will result in a spectrum of release times for charge de-trapping under reverse bias. The release time spectrum will consequently influence the temporal dependence of the reverse-bias signals which can in principle be analysed to elucidate the associated surface state energy distribution. Such an analysis would require signal data to be recorded over a more extensive range of time and temperature and is likely to be complicated by the inherent Gaussian spread (~0.1 eV [8]) of the DEH HOMO.

Conclusions

The properties of surface states in molecularly doped polymers may be investigated using simple thin-film diode structures where the injecting contact is used to initially charge the states before the trapped charge is extracted by reverse biasing the blocking contact. Applying this technique to HDPs has shown that the discharge characteristics of holes trapped in surface states are generally consistent with a leakage current that is driven by a surface electric field. The leakage current is sensitive to the concentration of the hydrazone dopant, but the surface states themselves are intrinsic to the polyester binder. Modelling of the leakage current suggests that the minimum concentration of HDP surface states is around 4×10^{12} cm^{-2} and that these states lie within about 17 Å of the film surface.

References

1. Street RA, Wong WS, Ready SE, Chabinyc IL, Arias AC, Limb S, Salleo A, Lujan R (2006) Mater Today 9:32
2. Makela T, Jussila S, Kosonen H, Backlund TG, Sandberg HGO, Stubb H (2005) Synth Met 153:285
3. Kololuoma T, Tuomikoski M, Makela T, Heilmann J, Haring T, Kallioinen J, Hagberg J, Kettunen I, Kopola H (2004) Emerg OptoElect Appl 5363:77
4. Goldie DM (2003) In: Nalwa HS (ed) Handbook of photochemistry and photobiology, vol 2. American Scientific Publishers, Steven Ranch, CA, p 195
5. Mort J, Pfister G, Grammatica S (1976) Solid State Comm 18:693
6. Mort J (1989) In: The anatomy of xerography: its invention and evolution. McFarland and Company, North Carolina and London, p 91
7. Goldie DM, Macartney AAW, Gibson RAG, Gairns RS (1997) Phil Mag B 75:553
8. Goldie DM (2006) J Non Cryst Solids 352:1648
9. Stolka M, Abkowitz MA (1993) Synth Metals 54:417
10. Chu TY, Song OK (2008) J Appl Phys 104:23711
11. Tyutnev AP, Saenko VS, Pozhidaev ED, Kolesnikov VA (2005) High Perf Poly 17:175
12. Tyutnev AP, Saenko VS, Pozhidaev ED, Ikhsanov RS (2008) J Phys Cond Matter 20:215219
13. Goldie DM (1999) J Phys D 32:3058
14. Abkowitz M, Bassler H, Stolka M (1991) Phil Mag B 63:201
15. Novikov SV, Dunalp DH, Kenkre VM, Parris PE, Vannikov AV (1998) Phys Rev Lett 81:4472
16. Mack JX, Schein LB, Peled A (1989) Phys Rev B 39:7500
17. Helfrich W, Mark P (1962) Z Physik 168:495
18. Street RA (1991) In: Hydrogenated amorphous silicon. Cambridge Solid State Science Series, Cambridge University Press, New York, p 75
19. Lampert MA, Mark P (1970) In: Current injection in solids. Academic Press, New York, p 42
20. Feller F, Rothe C, Tammer M, Geschke D, Monkman AP (2002) J Appl Phys 91:9225
21. Kaye GWC, Laby TH (1995) In: Tables of physical and chemical constants, Longman, London and New York, p 252
22. Kanemitsu Y, Imamura S (1990) J Appl Phys 67:3728
23. Zhang GJ, Yang K, Dong M, Zhao WB, Yan Z (2007) Appl Surf Sci 254:1450
24. Unni KNN, Dabos-Seignon S, Nunzi JM (2006) J Mater Sci 41:1865. doi:10.1007/s10853-006-7549-9
25. Torres I, Taylor DM (2005) J Appl Phys 98:73710
26. Yu CF, Lin DL, Sun X (1994) Phys Rev B 50:17120
27. Mizutani T, Takai Y, Osawa T, Ieda M (1976) J Phys D 9:2253
28. Duke CB (1978) Surf Sci 70:674